

# On the nature of rapidly fading Type II supernovae

Takashi J. Moriya<sup>1\*</sup>, Maria V. Pruzhinskaya<sup>2</sup>, Mattias Ergon<sup>3</sup>, and  
Sergei I. Blinnikov<sup>4,5,6</sup>

<sup>1</sup> *Argelander Institute for Astronomy, University of Bonn, Auf dem Hügel 71, D-53121 Bonn, Germany*

<sup>2</sup> *Lomonosov Moscow State University, Sternberg Astronomical Institute, Universitetsky pr., 13, Moscow, 119991, Russia*

<sup>3</sup> *The Oskar Klein Centre, Department of Astronomy, AlbaNova, Stockholm University, SE-10691 Stockholm, Sweden*

<sup>4</sup> *Institute for Theoretical and Experimental Physics, Bolshaya Cheremushkinskaya ulitsa 25, 117218 Moscow, Russia*

<sup>5</sup> *All-Russia Research Institute of Automatics, Sushchevskaya ulitsa 22, 127055 Moscow, Russia*

<sup>6</sup> *Kavli Institute for the Physics and Mathematics of the Universe (WPI), The University of Tokyo Institutes for Advanced Study, The University of Tokyo, 5-1-5 Kashiwanoha, Kashiwa, 277-8583 Chiba, Japan*

Accepted 2015 October 06. Received 2015 October 01; in original form 2015 May 26.

## ABSTRACT

It has been suggested that Type II supernovae with rapidly fading light curves (a.k.a. Type IIL supernovae) are explosions of progenitors with low-mass hydrogen-rich envelopes which are of the order of  $1 M_{\odot}$ . We investigate light-curve properties of supernovae from such progenitors. We confirm that such progenitors lead to rapidly fading Type II supernovae. We find that the luminosity of supernovae from such progenitors with the canonical explosion energy of  $10^{51}$  erg and  $^{56}\text{Ni}$  mass of  $0.05 M_{\odot}$  can increase temporarily shortly before all the hydrogen in the envelope recombines. As a result, a bump appears in their light curves. The bump appears because the heating from the nuclear decay of  $^{56}\text{Ni}$  can keep the bottom of hydrogen-rich layers in the ejecta ionized, and thus the photosphere can stay there for a while. We find that the light-curve bump becomes less significant when we make explosion energy larger ( $\gtrsim 2 \times 10^{51}$  erg),  $^{56}\text{Ni}$  mass smaller ( $\lesssim 0.01 M_{\odot}$ ),  $^{56}\text{Ni}$  mixed in the ejecta, or the progenitor radius larger. Helium mixing in hydrogen-rich layers makes the light-curve decline rates large but does not help reducing the light-curve bump. Because the light-curve bump we found in our light-curve models has not been observed in rapidly fading Type II supernovae, they may be characterized by not only low-mass hydrogen-rich envelopes but also higher explosion energy, larger degrees of  $^{56}\text{Ni}$  mixing, and/or larger progenitor radii than slowly fading Type II supernovae, so that the light-curve bump does not become significant.

**Key words:** supernovae: general — stars: massive — stars: mass-loss — stars: evolution

## 1 INTRODUCTION

Type II supernovae (SNe II) are SNe which show hydrogen features in their spectra (e.g., Filippenko 1997). It has been believed that they are explosions of massive stars which have kept their hydrogen-rich envelope until the time of the core collapse. Many direct detections of SN II progenitors, including the blue supergiant star in Sanduleak -69°202 exploded as SN 1987A, prove this idea (see Smartt 2009 for a review).

Even though SNe II commonly show hydrogen features in their spectra, their light-curve (LC) evolution is heterogeneous<sup>1</sup>. Classically, SN II LCs are classified in two distinct sub-classes, SNe IIP and IIL, based on their LCs. SNe IIP

show a LC “plateau” and their luminosity does not change much for about 100 days. On the contrary, the luminosity of SNe IIL constantly declines and their LCs look “linear”. While some studies suggest that these two sub-classes are distinct from each other (Arcavi et al. 2012; Faran et al. 2014a,b; Poznanski et al. 2015), others indicate that SNe IIP and IIL are not clearly separated and SN II LC decline rates have a continuous distribution (Anderson et al. 2014; Sanders et al. 2015). In this paper, we continue to use the word “SN IIL” to naively refer to SNe II whose LCs decline relatively rapidly. We note that it is not our intention to suggest that SNe IIL are a distinct class of SNe II when

\* moriyatk@astro.uni-bonn.de

<sup>1</sup> We do not consider SNe IIn in this paper because their LCs are

strongly affected by dense circumstellar media (e.g., Moriya et al. 2013).

**Table 1.** Progenitor properties.

$M_{\text{ZAMS}}$ $M_{\odot}$	$f$	$M_{\text{fin}}^a$ $M_{\odot}$	$M_{\text{env}}$ $M_{\odot}$	$X_{\text{surf}}^b$	$R$ $10^3 R_{\odot}$	$L^c$ $10^6 L_{\odot}$	$T_{\text{eff}}^d$ $10^3 \text{K}$
15	1.0	13.9	10.2	0.66	0.65	0.52	3.42
20	2.5	10.5	4.4	0.65	1.10	1.23	3.27
20	3.0	8.0	2.0	0.62	0.89	1.10	3.09
25	1.0	14.0	4.1	0.67	1.10	2.26	3.81
25	1.5	10.6	1.2	0.41	0.70	1.93	4.57

<sup>a</sup> Total mass, <sup>b</sup> Surface hydrogen abundance, <sup>c</sup> Luminosity, <sup>d</sup> Effective temperature

we say SNe IIL, nor to define SNe IIL. Some SNe II which we call SNe IIL in this paper may be classified as SNe IIP depending on how they are separated.

The primary origin of the diversity in the LC decline rates of SNe II are presumed to be in the remaining amount of hydrogen in the envelope (e.g., Grassberg, Imshennik, & Nadyozhin 1971; Falk & Arnett 1977; Litvinova & Nadezhin 1983; Swartz, Wheeler, & Harkness 1991; see also Blinnikov & Bartunov 1993; Young, Smith, & Johnson 2005). The luminosity of SNe II with less hydrogen-rich envelope masses declines more rapidly because of the low ejecta density (see also Goldfriend, Nakar, & Sari 2014; Pejcha & Prieto 2015b). If the hydrogen-rich envelope mass ( $M_{\text{env}}$ ) is sufficiently small, the SNe are observed as SNe IIB in which the spectral features transit from those of SNe II to SNe Ib (see Bufano et al. 2014 for a recent collection of SNe IIB). LC modeling of observed SNe indicates that the hydrogen-rich envelope masses of SN IIP progenitors are  $\sim 5 - 15 M_{\odot}$  (e.g., Popov 1993; Bersten, Benvenuto, & Hamuy 2011; Inserra et al. 2013; Utrobin & Chugai 2013; Pejcha & Prieto 2015a), while those of SN IIB progenitors are less than  $\sim 0.5 M_{\odot}$  (e.g., Shigeyama et al. 1994; Woosley et al. 1994; Blinnikov et al. 1998; Bersten et al. 2012; Ergon et al. 2014).

Most of SN II LC studies based on theoretical SN progenitors from stellar evolution have been performed for the progenitors with  $M_{\text{env}} \gtrsim 5 M_{\odot}$  which become SNe IIP (e.g., Kasen & Woosley 2009; Dessart, Livne, & Waldman 2010; Dessart & Hillier 2011; Dessart et al. 2013; Utrobin et al. 2015), and those with  $M_{\text{env}} \lesssim 0.5 M_{\odot}$  which become SNe IIB (e.g., Shigeyama et al. 1994; Woosley et al. 1994; Dessart et al. 2011, 2015). There exist only a few LC studies for the SN II progenitors with  $M_{\text{env}} \sim 1 M_{\odot}$  which are presumed to become rapidly fading SNe II or SNe IIL (Blinnikov & Bartunov 1993; Baklanov 2002; Young 2004; Dessart, Livne, & Waldman 2010; Morozova et al. 2015). In this paper, we focus on SN II progenitors with a hydrogen-rich envelope mass of  $\sim 1 M_{\odot}$  and perform a numerical LC study of such SN II progenitors. We investigate the nature of rapidly fading SNe II by numerically modeling LCs from such progenitors.

The rest of this paper is organized as follows. We introduce our progenitor models with  $M_{\text{env}} \sim 1 M_{\odot}$  in Section 2. We show LC models from our progenitors in Section 3. We discuss the nature of rapidly fading SNe II based on the obtained LC models in Section 4. We conclude this paper in Section 5.

## 2 PROGENITORS WITH LOW-MASS HYDROGEN-RICH ENVELOPES

We use a public stellar evolution code **MESASstar** version 6794 (Paxton et al. 2011, 2013, 2015) to obtain SN progenitors with low-mass hydrogen-rich envelopes. We evolve stars with the zero-age main-sequence (ZAMS) masses ( $M_{\text{ZAMS}}$ ) of 15, 20, and 25  $M_{\odot}$ . The initial metallicity is assumed to be  $Z = 0.02$ . The stellar evolution is followed until the core collapse, except for one model specified below. Convection is treated with the mixing-length theory with a mixing-length parameter of 1.6. The Ledoux criterion for convection is adopted with a semiconvective efficiency of 1.0. No overshooting is taken into account.

We obtain several SN progenitors with low-mass hydrogen-rich envelopes by changing their mass-loss rates. The standard mass-loss rates  $\dot{M}_{\text{st}}$  are the ‘‘Dutch’’ mass-loss rates adopted in **MESASstar**. The standard mass-loss rates for stars with the effective temperature higher than  $10^4 \text{ K}$  are based on Vink, de Koter, & Lamers (2001). Those for stars cooler than  $10^4 \text{ K}$  are from de Jager, Nieuwenhuijzen, & van der Hucht (1988). The actual mass-loss rates ( $\dot{M}$ ) used in our calculations are

$$\dot{M} = f \dot{M}_{\text{st}}. \quad (1)$$

The factor  $f$  is made as large as 3 in this study. The observed mass-loss rates scatter more than by a factor of 3, and the adopted mass-loss rates are within uncertainties (e.g., Meynet et al. 2015).

Table 1 summarizes the properties of the SN progenitors we have numerically evolved for this study. We obtain four stars with  $M_{\text{env}}$  between 1 and 5  $M_{\odot}$ . We also obtain a star with  $M_{\text{env}} = 10.2 M_{\odot}$  ( $M_{\text{ZAMS}} = 15 M_{\odot}$ ) for comparison. The evolution of the star with  $M_{\text{ZAMS}} = 20 M_{\odot}$  and  $f = 3.0$  is only followed up to the end of the core Ne burning. However, the star is expected to explode within several years after the core Ne burning and the envelope structure and the final mass are not likely to be affected in the remaining time to the core collapse. The other stars are evolved until the core collapse.

## 3 LIGHT CURVES

We perform numerical LC calculations for the SN progenitors described in the previous section. We use a one-dimensional multi-frequency radiation hydrodynamics code **STELLA** to follow LCs numerically (e.g., Blinnikov & Bartunov 1993; Blinnikov et al. 1998, 2006). We take the central  $1.4 M_{\odot}$  of the SN progenitors away

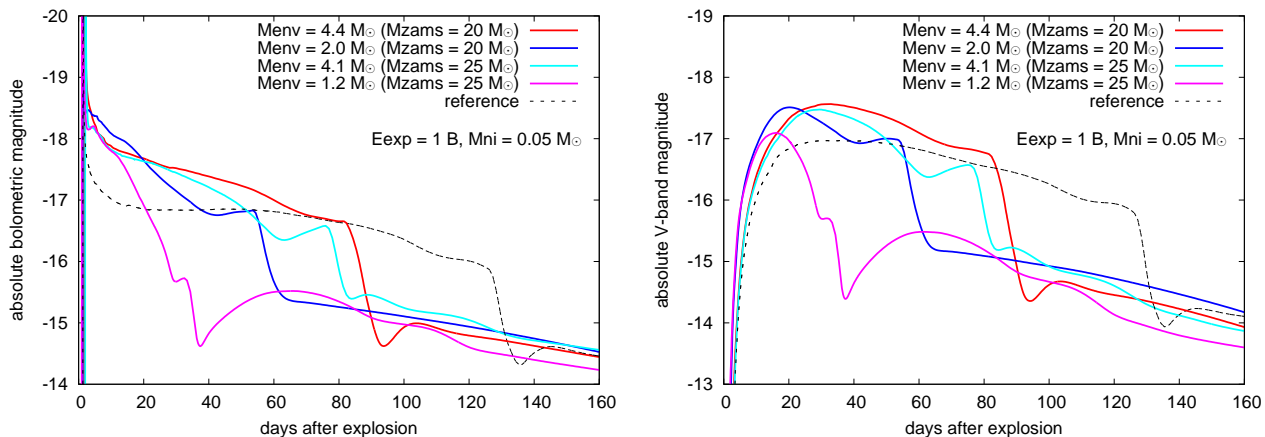


**Figure 1.** Bolometric (left) and V-band (right) LCs from our progenitors with low-mass hydrogen-rich envelopes exploded with the canonical explosion energy (1 B) and  $^{56}\text{Ni}$  mass ( $0.05 M_{\odot}$ ). The reference LC are from our  $15 M_{\odot}$  progenitor model.

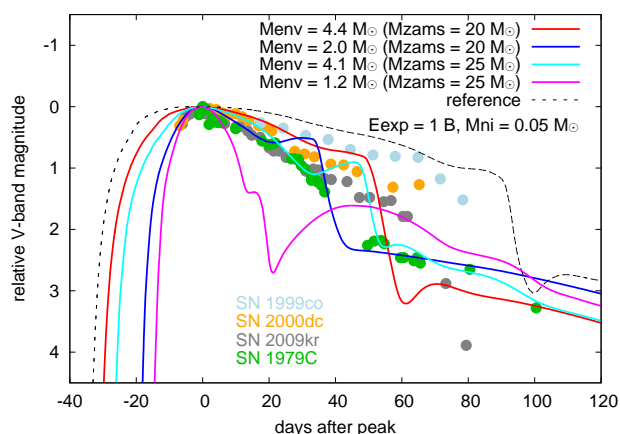


**Figure 2.** V-band LCs of our canonical explosion models scaled at the LC peak. The V-band LCs of SNe II with several LC decline rates are also presented. The observational data are from Faran et al. (2014b) (SNe 1999co and 2000dc), Elias-Rosa et al. (2010) (SN 2009kr), and de Vaucouleurs et al. (1981) (SN 1979C). SNe 2009kr and 1979C are among the most rapidly fading SNe II (e.g., Faran et al. 2014b; Anderson et al. 2014).

for the LC calculations, assuming that the central region becomes a neutron star. SN explosions are initiated by putting thermal energy to the innermost layers. We do not follow the explosive nucleosynthesis. Thus, the SN ejecta composition is the same as the pre-SN composition except for  $^{56}\text{Ni}$ . When we do not take mixing into account,  $^{56}\text{Ni}$  is located at the center of SN ejecta. When we mix  $^{56}\text{Ni}$  (Section 3.3),  $^{56}\text{Ni}$  is evenly mixed within the mixed region. We also investigate the effect of helium mixing into the hydrogen-rich envelope (Section 3.4). As our focus in this paper is on the early LCs when the photosphere is located in the hydrogen-rich envelopes, the effect of the explosive nucleosynthesis on our results is presumed to be small.

### 3.1 Canonical explosion energy and $^{56}\text{Ni}$ mass

We adopt an explosion energy of  $10^{51} \text{ erg} \equiv 1 \text{ B}$  and a  $^{56}\text{Ni}$  mass of  $0.05 M_{\odot}$  as the canonical values based on the observations of SNe II (e.g., Hamuy 2003; Anderson et al. 2014; Sanders et al. 2015).  $^{56}\text{Ni}$  is located at the center of the ejecta in the canonical models, although SNe II are known to be affected by mixing (e.g., Arnett et al. 1989). The effect of mixing is discussed in the later sections.

Figure 1 presents our LCs with the canonical explosion parameters. The reference LC is from our  $M_{\text{ZAMS}} = 15 M_{\odot}$  model which has  $M_{\text{env}} = 10.2 M_{\odot}$ . The bolometric luminosity does not change significantly for more than 50 days when the recombination wave travels in the hydrogen-rich envelope. Then, the LC drops when the recombination wave disappears from the hydrogen-rich envelope. The V-band LC decline rate after the peak before the drop is  $0.48 \text{ mag day}^{-1}$ . We see rebrightening after the LC drop before the LC start to follow the nuclear decay. In this phase, the SN have already entered the nebular phase. Our code is not suitable to follow the nebular phase and this rebrightening may be a numerical artifact.

The early luminosity in the LC models with  $M_{\text{env}} \sim 1 M_{\odot}$  is brighter than that of the reference LC because of the lower envelope masses (e.g., Kasen & Woosley 2009). In Fig. 2, we show the V-band LCs scaled with their peak magnitudes. We can find that SN II progenitors with low-mass hydrogen-rich envelopes result in rapidly fading SNe II as expected from previous studies. We also show the observed V-band LCs for SNe II with relatively large decline rates. We can see that our low-mass envelope progenitors provide LC decline rates consistent with the observations. Especially, the V-band LC decline rates for our models with  $M_{\text{env}} = 2.0 M_{\odot}$  and  $4.1 M_{\odot}$  are consistent with those of SNe 2009kr and 1979C, which are among the most rapidly fading SNe II and often referred as SNe IIL.

Looking into the LC of SN 2009kr as an example, a substantial LC drop is observed at around 60 days after the peak. This kind of the LC drop is observed in several rapidly fading SNe (e.g., Valenti et al. 2015). The LC drop caused by the recombination wave reaching the bottom of the hydrogen-rich envelope in the model with  $M_{\text{env}} = 4.1 M_{\odot}$  is

found at around 50 days after the peak and there is only a difference of about 10 days.

A significant difference between our numerical LCs and observed ones is in the existence of a period of a slight luminosity increase between the early fading phase and the LC drop. The bolometric luminosity increase is found in three of our canonical models. The luminosity increase is also found in the *V*-band LCs, although the increase in the *V*-band LC with  $M_{\text{env}} = 1.2 M_{\odot}$  is less significant and it is almost flat. The remaining LC with  $M_{\text{env}} = 4.4 M_{\odot}$  does not show the luminosity increase, but the LC flattens before the drop. We call the increasing part of the LCs we found in our LC models as a “bump” in the following. We clearly see the LC bump in the models with  $M_{\text{env}} = 4.1$  and  $2.0 M_{\odot}$ , while it is vague in the model with  $M_{\text{env}} = 4.4 M_{\odot}$ . The model with  $M_{\text{env}} = 1.2 M_{\odot}$  shows the bump in a short timescale. Thus, we are likely to observe the LC bump for a long time in the canonical explosions of the progenitors with  $M_{\text{env}} \simeq 2 - 4 M_{\odot}$ . This kind of bumps are also found in other numerical LC models of rapidly fading SNe II (e.g., Swartz, Wheeler, & Harkness 1991; Baklanov 2002; Young 2004), but they are not paid attention much. The origin of the bump is discussed in the next section where LC models with different  $^{56}\text{Ni}$  masses and explosion energies are presented. In this study, we focus on this bump and try to use it to deduce the nature of rapidly fading SNe II.

Another LC feature to note is in our LC model of the smallest  $M_{\text{env}}$  ( $M_{\text{env}} = 1.2 M_{\odot}$ ). Because the recombination wave recedes in the hydrogen-rich envelope very quickly due to the small  $M_{\text{env}}$ , the early LC declines in a very short timescale. Then, after the LC drop following the bump discussed above, the luminosity increases again instead of following the  $^{56}\text{Co}$  nuclear decay rate. The peak time of this part of the LC ( $\sim 60$  days) corresponds to the diffusion time in the core, and thus the luminosity increase is likely due to the diffusion in the core. The hydrogen-rich envelope mass in the model is close to those in SNe I Ib and the LC starts to be similar to those of SNe I Ib with  $M_{\text{env}} = 1.2 M_{\odot}$ . The bolometric LC shape is also somewhat similar to that of SN 1987A, although our LC evolves in shorter timescales (e.g., Suntzeff et al. 1992). This kind of SNe II may exist as an intermediate type between SNe I IL and SNe I Ib.

### 3.2 Other explosion energies and $^{56}\text{Ni}$ masses

To investigate the cause of the LC bump found in our rapidly fading SN II models, we explore LCs with different explosion energies and  $^{56}\text{Ni}$  masses in this section. For this purpose, we use the  $14.0 M_{\odot}$  progenitor model with  $M_{\text{env}} = 4.1 M_{\odot}$  ( $M_{\text{ZAMS}} = 25 M_{\odot}$ ). We choose this model for our further investigation because (i) the LC from the canonical explosion parameters has a significant bump, (ii) the progenitor has almost the same mass as our reference model ( $14 M_{\odot}$ ), and (iii) the progenitor is obtained without modifying the mass-loss rates ( $f = 1.0$ ). General bump properties found for this progenitor model with different explosion energies and  $^{56}\text{Ni}$  masses are also found in other progenitors. We use three different explosion energies (1, 2, and 3 B) and  $^{56}\text{Ni}$  masses (0.01, 0.05, and  $0.1 M_{\odot}$ ).

Figure 3 shows the LCs with different explosion energies and  $^{56}\text{Ni}$  masses. First of all, we find that the bump is strongly affected by the  $^{56}\text{Ni}$  mass. When the  $^{56}\text{Ni}$  mass

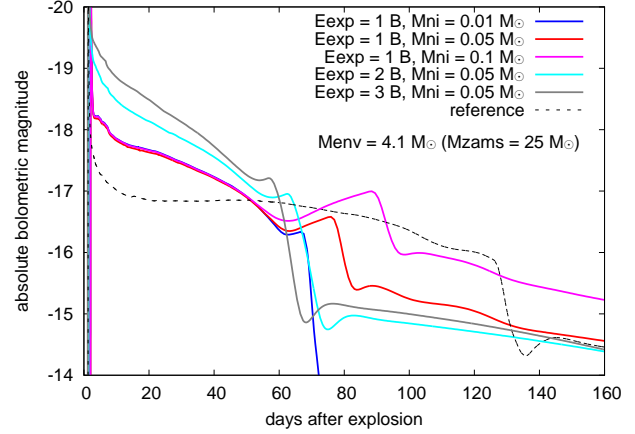


**Figure 3.** Bolometric LCs from the explosions of our progenitor model with  $M_{\text{env}} = 4.1 M_{\odot}$  with different explosion energies and  $^{56}\text{Ni}$  masses. The reference LC is the same as in Fig. 1.

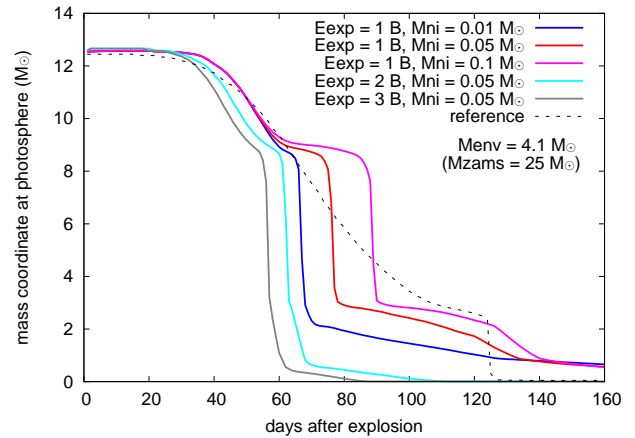


**Figure 4.** Evolution of the location of photosphere in our LC models presented in Fig. 3.

is increased to  $0.1 M_{\odot}$ , the duration of the bump becomes twice as long as that of the model with  $M_{^{56}\text{Ni}} = 0.05 M_{\odot}$ . When the  $^{56}\text{Ni}$  mass is decreased to  $0.01 M_{\odot}$ , the LC bump almost disappears and there only remains a brief almost plateau phase after the early declining phase. In the case of SNe I IP, the amount of  $^{56}\text{Ni}$  affects the duration of the plateau phase, but we do not expect the formation of the bump in this  $^{56}\text{Ni}$  mass range (Kasen & Woosley 2009). Dessart, Livne, & Waldman (2010) presented a LC model with  $M_{\text{env}} = 2.2 M_{\odot}$ , but they did not include  $^{56}\text{Ni}$ . This may be why they did not find the bump in their LC.

The fact that the LC bump is strongly affected by the  $^{56}\text{Ni}$  mass indicates that the LC bump is caused by the heating from the nuclear decay of  $^{56}\text{Ni} \rightarrow ^{56}\text{Co} \rightarrow ^{56}\text{Fe}$ . In Fig. 4, we show the location of the photosphere in the models presented in Fig. 3. Photosphere is defined as the location where the Rosseland mean optical depth becomes  $2/3$ . The photosphere recedes inward similarly at first in the models with different  $^{56}\text{Ni}$  masses. Then, when the photosphere reaches near the bottom of the hydrogen-rich envelope, the photosphere stays there for a while because the heating due to



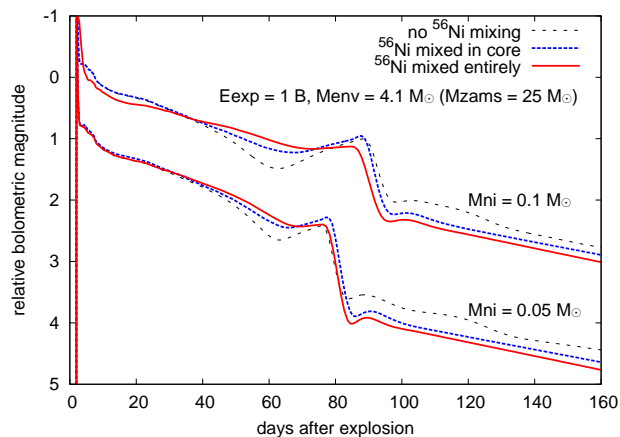


**Figure 5.** Bolometric LCs with different degrees of  $^{56}\text{Ni}$  mixing. The effect of the mixing is explored with the explosions of the  $M_{\text{env}} = 4.1 M_{\odot}$  progenitor with the canonical explosion energy (1 B) and two different  $^{56}\text{Ni}$  masses ( $0.05 M_{\odot}$  and  $0.1 M_{\odot}$ ). The models with the same  $^{56}\text{Ni}$  mass are scaled with the same magnitude.

the nuclear decay can keep hydrogen ionized. Because the radius of the photosphere increases with time if it stays in the same mass coordinate, the luminosity increases during this epoch. Thus, the bump appears in the LCs. The photosphere eventually goes into the core when hydrogen in the envelope can no longer be kept ionized, and the LCs drop at that moment. Because larger amount of  $^{56}\text{Ni}$  can keep hydrogen ionized longer, the bump appears more significantly with larger amount of  $^{56}\text{Ni}$ .

Next, we investigate the effect of explosion energy. Figure 3 shows LCs with different explosion energies. The evolution of the location of the photosphere is in Fig. 4. The early luminosity becomes larger as the explosion energy increases. Meanwhile, the bump is significantly reduced or almost disappears when the explosion energy is above 2 B when  $M_{^{56}\text{Ni}} = 0.05 M_{\odot}$ . This is because more rapid expansion results in more rapid reduction of the gamma-ray optical depth, and the heating from the nuclear decay is less effective. In addition, the adiabatic cooling in the SN ejecta becomes more effective with higher explosion energy. As a result, the photosphere no longer stays at the bottom of the hydrogen-rich layers for a long time. The LC models in Blinnikov & Bartunov (1993) do not have significant bumps presumably because they mostly present LCs for an explosion energy of 2 B.

To summarize, we find that large explosion energies ( $E_{\text{exp}} \gtrsim 2 \text{ B}$ ) and small  $^{56}\text{Ni}$  masses ( $M_{^{56}\text{Ni}} \lesssim 0.01 M_{\odot}$ ) make the LC bumps less significant.

### 3.3 $^{56}\text{Ni}$ mixing

In all the models presented so far,  $^{56}\text{Ni}$  is placed at the center of SN ejecta. We find that the heating from the nuclear decay of  $^{56}\text{Ni}$  strongly affects the LC bump in the previous section. Since the heating from the nuclear decay depends on the degree of the  $^{56}\text{Ni}$  mixing, we investigate the effect of the  $^{56}\text{Ni}$  mixing on the LC bumps. We assume two kinds of  $^{56}\text{Ni}$  mixing in our LC calculations.  $^{56}\text{Ni}$  is mixed only in

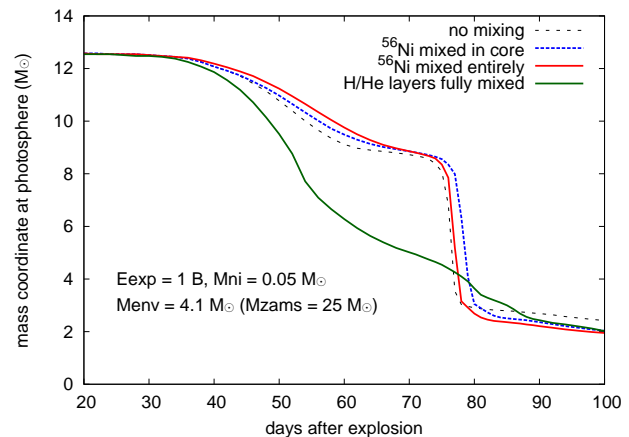


**Figure 6.** Evolution of the location of photosphere in the LC models with different mixing presented in Figs. 5 and 7.

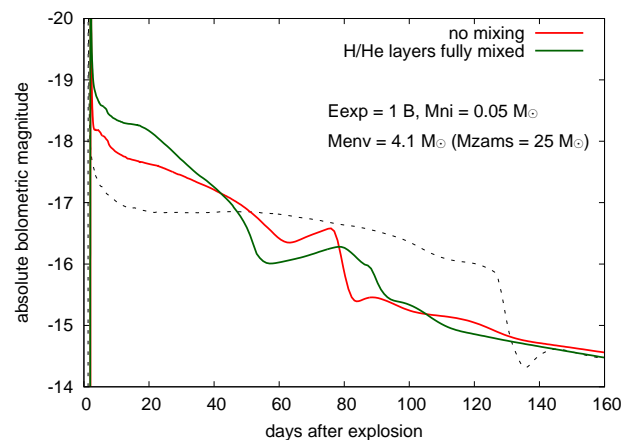


**Figure 7.** Bolometric LC from the progenitor in which hydrogen-rich and helium layers are fully mixed.

the core in one case and in the entire SN ejecta in the other.  $^{56}\text{Ni}$  is uniformly mixed in both cases.

Figure 5 shows how the LC bump is affected by the  $^{56}\text{Ni}$  mixing. The higher degree of mixing makes the LC bump less significant. This is because the photosphere recedes more slowly with the  $^{56}\text{Ni}$  mixing thanks to the more efficient heating by the nuclear decay in the outer hydrogen-rich layers. The slower recession of the photosphere can be seen in Fig. 6 where the evolution of photosphere in mass coordinate is shown.

Another interesting consequence of the  $^{56}\text{Ni}$  mixing appears in the late-time LC tails after the luminosity drop. All the late-time LCs decline with the timescale of the  $^{56}\text{Co}$  decay. Meanwhile, the luminosity of the tails depends on the degree of the  $^{56}\text{Ni}$  mixing. This is simply because gamma-rays from the nuclear decay are less likely to be absorbed by the ejecta if they are emitted in outer layers. Recently, Wheeler, Johnson, & Clocchiatti (2015) argued that the LC tails of Type IIb/Ib/Ic SNe have much diversity even if their early LCs have similar properties. They ascribed the diversity on the explosion asymmetry. However, the difference in the degree of the  $^{56}\text{Ni}$  mixing, which is not considered in

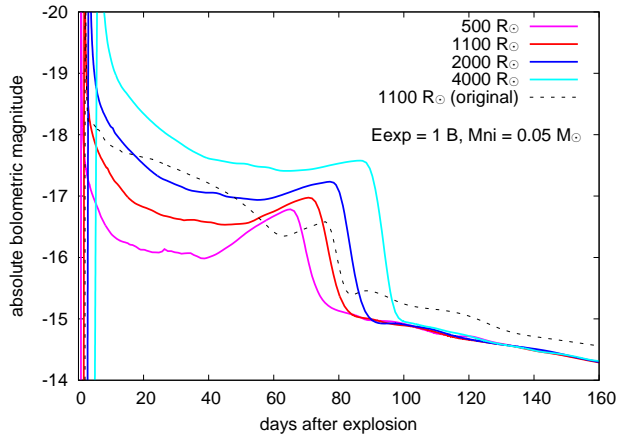


**Figure 8.** Bolometric LCs from simplified progenitors with different radii. We also show the original model with the same mass ( $M_{\text{fin}} = 14.0 M_{\odot}$  and  $M_{\text{env}} = 4.1 M_{\odot}$ ) whose radius is  $1100 R_{\odot}$ .

the analytic LC model of Arnett (1982) they use, can also make the diversity in the late-time LCs (see also Ergon et al. 2014).

### 3.4 Helium mixing

Multi-dimensional simulations of stellar explosions show that the hydrogen-rich layer and helium core are mixed during the explosion because of the Rayleigh-Taylor instability (e.g., Hachisu et al. 1990). The mixing of helium into the hydrogen-rich layers affects the LC shape (e.g., Woosley 1988; Shigeyama & Nomoto 1990; Utrobin 2007). It is also suggested that the helium mixing in the hydrogen-rich layers can result in the rapid declines in SNe II (e.g., Swartz, Wheeler, & Harkness 1991). We investigate the effect of the helium mixing in the hydrogen-rich layer on the LC bump.

Our progenitor model with  $M_{\text{env}} = 4.1 M_{\odot}$  has helium mass of  $6.4 M_{\odot}$  and hydrogen mass of  $3.1 M_{\odot}$  in total in hydrogen-rich and helium layers. Based on this progenitor model, we construct a progenitor model in which the hydrogen-rich and helium layers are fully mixed. Thus, the model has  $9.5 M_{\odot}$  of the mixed outer layer with the hydrogen fraction of 0.33 and the helium fraction of 0.67.

The LC from the mixed progenitor is presented in Fig. 7. As is found in previous studies, the higher helium fraction in the envelope due to the helium mixing makes the early LC brighter (e.g., Swartz, Wheeler, & Harkness 1991; Kasen & Woosley 2009). The higher helium fraction makes the recombination temperature higher, and it results in the fast recession of the recombination front (Fig. 6). However, the heating from the nuclear decay can still keep the innermost layers of the mixed envelope ionized. Thus, the helium mixing does not result in the reduction nor disappearance of the LC bump. The duration of the LC bump with the helium mixing actually gets longer than that without the helium mixing, because the photosphere travels faster than in the model without mixing and it reaches the bottom of the mixed layer earlier.

### 3.5 Progenitor radii

Radii of SN II progenitors change their LC shapes (e.g., Young 2004). The LC models presented so far are based on the progenitors developed with MESAR, and thus our progenitor radii are based on the stellar structure obtained by the code. However, there are uncertainties in the stellar evolution theory, and the stellar radii obtained by the code have uncertainties. Dessart et al. (2013) suggested that SNe IIP progenitors may have smaller radii than those predicted by the stellar evolution theory based on their LC models (see also González-Gaitán et al. 2015), while violent nuclear burning at the stellar core in the final stages of the stellar evolution may result in the stellar surface expansion (e.g., Quataert & Shiode 2012; McIey & Soker 2014; Moriya 2014). We investigate how the uncertainties in the progenitor radii affect the LC bump in this section.

We use simplified stellar structure to obtain SN II progenitors with different radii. We keep the progenitor and envelope mass the same as the original model with  $M_{\text{fin}} = 14.0 M_{\odot}$  and  $M_{\text{env}} = 4.1 M_{\odot}$  developed from  $M_{\text{ZAMS}} = 25 M_{\odot}$  which has the progenitor radius  $R = 1100 R_{\odot}$ . The stellar structure is constructed based on the polytropic equation of state with the polytropic index of 3 (see, e.g., Blinnikov & Bartunov 1993; Baklanov 2002 for details). The stellar interior abundance is kept the same as in the original model. We explode the progenitor with the canonical explosion energy (1 B) and  $^{56}\text{Ni}$  mass ( $0.05 M_{\odot}$ ) without any mixing.

In Fig. 8, we show the LC models from the progenitors with different radii and the original model from MESAR. Although the original model and the artificial model with the same radius ( $1100 R_{\odot}$ ) have different early LC evolution because of the difference in the density structure, the LC bump is still found in both models. The LC bump becomes less significant in larger progenitors. This is because the early luminosity during the plateau phase is brighter when the progenitor is larger (e.g., Kasen & Woosley 2009). The effect of the temporal luminosity increase is less significant because of the higher early luminosity caused by the larger progenitor radii.

## 4 DISCUSSION

### 4.1 Photospheric velocity

We have focused on the LC properties from the explosions of the progenitors with hydrogen-rich envelope mass of  $\sim 1 M_{\odot}$ . For the completeness, we show the photospheric velocities of the models we have presented so far. Photospheric velocities affect the spectral properties of SNe, and the information on photospheric velocities is complementary to the LC properties.

Figure 9 shows the photospheric velocities of our models. They are within those estimated in rapidly fading SNe II (e.g., Faran et al. 2014b). Our rapidly fading SN II models typically have higher photospheric velocities than the reference model, as is observed in rapidly fading SNe II (e.g., Faran et al. 2014b). This is because of the lower envelope mass in the rapidly fading SNe II. The photospheric velocities are mainly affected by the explosion energy and the helium mixing in a given progenitor model.

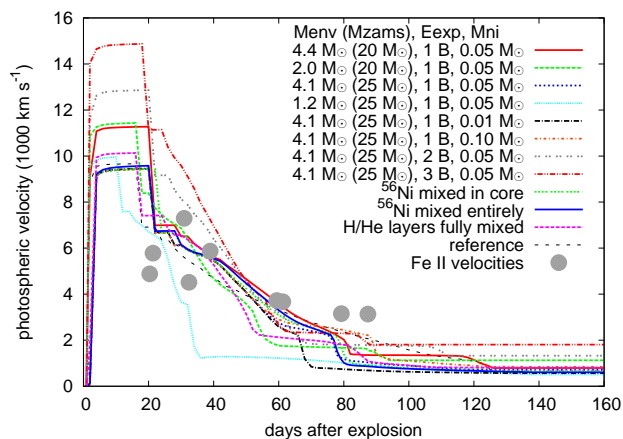


**Figure 9.** Photospheric velocities of the explosion models presented in this study. The collection of Fe II velocities observed in rapidly fading SNe II presented in Faran et al. (2014b) scaled with a typical observed photospheric velocity at 50 days ( $4000 \text{ km s}^{-1}$ , e.g., Poznanski et al. 2015) is shown for comparison.

## 4.2 Nature of rapidly fading SNe II indicated from the LC bump

Based on the LC models obtained so far, we discuss the nature of rapidly fading SNe II. We have confirmed that SNe II from progenitors with low-mass hydrogen-rich envelopes fade quickly, and their decline rates are consistent with those observed in rapidly fading SNe II. However, our LC models with the canonical explosion energy ( $E_{\text{exp}} = 1 \text{ B}$ ) and  $^{56}\text{Ni}$  mass ( $M_{^{56}\text{Ni}} = 0.05 \text{ M}_{\odot}$ ) often show a temporal luminosity increase (LC bump) before all the hydrogen in the hydrogen-rich envelope recombines. This kind of LC bumps have not been observed in rapidly fading SNe II. This implies that rapidly fading SNe II may not only be characterized by low-mass hydrogen-rich envelopes. Some explosion properties which prevent LCs from having the LC bump may be commonly shared among rapidly fading SNe II.

We have found four possible ways to make the LC bump less significant, i.e., large explosion energies ( $E_{\text{exp}} \gtrsim 2 \text{ B}$ ), small  $^{56}\text{Ni}$  masses ( $M_{^{56}\text{Ni}} \lesssim 0.01 \text{ M}_{\odot}$ ), large degrees of  $^{56}\text{Ni}$  mixing, and large progenitor radii. If SN II progenitors with low-mass hydrogen-rich envelopes tend to come from relatively more massive stars among SN II progenitors, they are likely to have larger explosion energy, according to the empirical relation between explosion energy and progenitor mass (e.g., Hamuy 2003; Nomoto et al. 2011; Utrobin & Chugai 2013; Poznanski 2013; Pejcha & Prieto 2015a; Bose et al. 2015). Then, the lack of the LC bump may indicate that most rapidly fading SNe II have low-mass hydrogen-rich envelopes because of higher ZAMS masses, which end up with both low-mass hydrogen-rich envelopes and high explosion energies. SN II progenitors with low-mass hydrogen-rich envelopes can also originate from small ZAMS mass stars if they are in binary systems thanks to the mass loss by binary interactions (e.g., Nomoto, Iwamoto, & Suzuki 1995; Eldridge, Izzard, & Tout 2008). However, small ZAMS mass SN IIL progenitors are disfavored if SNe IIL typically have larger explosion energies than SNe IIP, contrary to SNe IIB

which may prefer small ZAMS mass progenitors in binary systems (e.g., Benvenuto, Bersten, & Nomoto 2013; Folatelli et al. 2014; Jerkstrand et al. 2015). There are other observational indications that SNe IIL may prefer higher ZAMS mass progenitors than SNe IIP (e.g., Elias-Rosa et al. 2011; Anderson et al. 2012; Kuncarayakti et al. 2013, see Maund et al. 2015 for the case of SN 2009kr).

A small amount of  $^{56}\text{Ni}$  in the ejecta is also shown to reduce the LC bump. However, SN II observations indicate that rapidly fading SNe II tend to have slightly higher  $^{56}\text{Ni}$  masses than slowly fading ones (Anderson et al. 2014). Thus, observations disfavor this way of making the LC bump less significant, although several possible mechanisms can make  $^{56}\text{Ni}$  masses of SNe II small. For example, some high mass progenitors may suffer significantly from fallback, resulting in small amount of  $^{56}\text{Ni}$  ejection.

The LC bump is also shown to be reduced by large degrees of the  $^{56}\text{Ni}$  mixing. Some SNe II are suggested to experience significant mixing in the SN ejecta (e.g., SN 1987A, Arnett et al. 1989). The lack of the LC bump in observed SNe II may thus indicate that SNe II generally have large degrees of internal mixing, dredging up  $^{56}\text{Ni}$  above the stellar core.

It has been suggested that the rapidly fading SNe II may result from the larger degree of helium mixing (e.g., Swartz, Wheeler, & Harkness 1991). We have confirmed that the helium mixing does make the LC decline rate of SNe II larger. However, the helium mixing does not result in the reduction of the LC bump. The fact that we do not observe the LC bump indicates that the helium mixing is not the only reason we observe rapidly fading SNe II. Even if the helium mixing plays a role in having a large decline rate, other mechanisms like the  $^{56}\text{Ni}$  mixing should be accompanied to reduce the LC bump.

Finally, radii of SN II progenitors may be significantly expanded, as we discussed in Section 3.5. The expansion of the progenitor radii can result in large luminosity, which makes the LC bump less significant, and reduction of the hydrogen-rich envelope density (e.g., McIey & Soker 2014), which makes the LC decline more rapid. In addition, the radius expansion of SNe II progenitors with large  $M_{\text{env}}$  may also result in rapidly fading SNe II with SN IIP features like ASASSN-13co (Holoien et al. 2014) because of the small envelope density with a large hydrogen-rich envelope mass. The observed rise times of SNe II are suggested to indicate smaller progenitor radii for more rapidly fading SNe II, but the difference may not be significant (Gall et al. 2015; González-Gaitán et al. 2015). The shock breakout observations as is recently reported by Tominaga et al. (2015) will further help to constrain the progenitor radii.

To summarize, the LC bumps we find in our LC models for the progenitors with low-mass hydrogen-rich envelopes which is not observed in SN IIL LCs indicates that rapidly fading SNe II are not only characterized by a low-mass hydrogen-rich envelope, which is responsible for the rapid LC decline, but also by explosion properties, large degrees of  $^{56}\text{Ni}$  mixing, and/or large progenitor radii. The later two properties, the large  $^{56}\text{Ni}$  mixing and large progenitor radii may also be a general characteristic of SNe II including SNe IIP, but their consequences may simply be easier to recognize in rapidly fading SNe II.

## 5 CONCLUSIONS

We have presented our results of LC modeling of SNe II from progenitors with hydrogen-rich envelope masses near the solar mass. We have confirmed that this kind of SN progenitors result in rapidly fading SNe II (SNe IIL). However, we find that theoretical LCs from such SN progenitors show a temporal luminosity increase (LC bump) shortly before all the hydrogen in the envelope recombines when they have the canonical explosion energy of 1 B and  $^{56}\text{Ni}$  mass of  $0.05 M_{\odot}$ . The temporal luminosity increase is due to the heating from the  $^{56}\text{Ni}$  decay, which keeps hydrogen ionized and make the photosphere stay at the innermost layers of the hydrogen-rich envelope for a while. Because this kind of temporal luminosity increase has not been observed, rapidly fading SNe II are likely to have more properties in common than a low-mass hydrogen-rich envelope, making the LC bump less significant.

We show four possible ways to make the LC bump less significant, i.e.,

- (i) large explosion energies ( $E_{\text{exp}} \gtrsim 2 \text{ B}$ )
- (ii) small  $^{56}\text{Ni}$  masses ( $M_{^{56}\text{Ni}} \lesssim 0.01 M_{\odot}$ )
- (iii) large degrees of  $^{56}\text{Ni}$  mixing
- (iv) extended progenitor radii.

We also find that the helium mixing into the hydrogen-rich layer does not help reducing the LC bump, although it can make LC decline rates large.

Because rapidly fading SNe II are observationally found to have larger  $^{56}\text{Ni}$  masses than slowly fading SNe II (Anderson et al. 2014), the lack of the LC bump in observed SN IIL LCs indicates that the other three properties are likely to be shared among SNe IIL, in addition to the low-mass hydrogen-rich envelope. If SN IIL progenitors tend to have larger explosion energies than those of SNe IIP, the empirical relation between the progenitor mass and the explosion energy implies that SN IIL progenitors are more massive than SN IIP progenitors. Then, most of SN IIL progenitors may not originate from small ZAMS mass progenitors which can lose their hydrogen-rich envelope by binary interactions. Alternatively, SNe IIL may have larger degrees of  $^{56}\text{Ni}$  mixing or more extended progenitor radii than expected.

Another possible way to interpret the lack of the LC bump in SNe IIL is that not only SNe IIL but SNe II including SNe IIP may generally have large degrees of  $^{56}\text{Ni}$  mixing and/or extended progenitor radii. The effect of large  $^{56}\text{Ni}$  mixing and an extended progenitor radius may be easier to recognize in SN progenitors with low-mass hydrogen-rich envelopes through the LC bump as we find in this study. Constraining the degree of the  $^{56}\text{Ni}$  mixing and the expansion of the progenitor radius in SNe IIL as well as SNe IIP will be helpful to further constrain the intrinsic properties of SNe IIL.

## ACKNOWLEDGMENTS

TJM is supported by Japan Society for the Promotion of Science Postdoctoral Fellowships for Research Abroad (26-51). Pruzhinskaya M.V. is supported by the Russian Foundation of Fundamental Research, grant RFFI 14-02-31546 and by Mechnikov Scholarship of the Embassy of France. This work

of S. I. Blinnikov (development of STELLA code) was supported by Russian Science Foundation grant 14-12-00203. Numerical computations were partially carried out on Cray XC30 and PC cluster at Center for Computational Astrophysics, National Astronomical Observatory of Japan. The Oskar Klein Centre is funded by the Swedish Research Council. This research is also supported by World Premier International Research Center Initiative (WPI Initiative), MEXT, Japan.

## REFERENCES

- Anderson J. P., et al., 2014, *ApJ*, 786, 67  
 Anderson J. P., Habergham S. M., James P. A., Hamuy M., 2012, *MNRAS*, 424, 1372  
 Arcavi I., et al., 2012, *ApJ*, 756, L30  
 Arnett W. D., 1982, *ApJ*, 253, 785  
 Arnett W. D., Bahcall J. N., Kirshner R. P., Woosley S. E., 1989, *ARA&A*, 27, 629  
 Baklanov P. V., 2002, Dissertation, Lomonosov Moscow State University (<http://www.astronet.ru/db/msg/1174722/index.html>)  
 Benvenuto O. G., Bersten M. C., Nomoto K., 2013, *ApJ*, 762, 74  
 Bersten M. C., Benvenuto O., Hamuy M., 2011, *ApJ*, 729, 61  
 Bersten M. C., et al., 2012, *ApJ*, 757, 31  
 Blinnikov S. I., Bartunov O. S., 1993, *A&A*, 273, 106  
 Blinnikov S. I., Eastman R., Bartunov O. S., Popolitov V. A., Woosley S. E., 1998, *ApJ*, 496, 454  
 Blinnikov S. I., Popov D. V., 1993, *A&A*, 274, 775  
 Blinnikov S. I., Röpke F. K., Sorokina E. I., Gieseler M., Reinecke M., Travaglio C., Hillebrandt W., Stritzinger M., 2006, *A&A*, 453, 229  
 Bose S., et al., 2015, *ApJ*, 806, 160  
 Bufano F., et al., 2014, *MNRAS*, 439, 1807  
 de Jager C., Nieuwenhuijzen H., van der Hucht K. A., 1988, *A&AS*, 72, 259  
 Dessart L., Hillier D. J., 2011, *MNRAS*, 410, 1739  
 Dessart L., Hillier D. J., Livne E., Yoon S.-C., Woosley S., Waldman R., Langer N., 2011, *MNRAS*, 414, 2985  
 Dessart L., Hillier D. J., Waldman R., Livne E., 2013, *MNRAS*, 433, 1745  
 Dessart L., Hillier D. J., Woosley S., Livne E., Waldman R., Yoon S.-C., Langer N., 2015, *arXiv*, arXiv:1507.07783  
 Dessart L., Livne E., Waldman R., 2010, *MNRAS*, 408, 827  
 de Vaucouleurs G., de Vaucouleurs A., Buta R., Ables H. D., Hewitt A. V., 1981, *PASP*, 93, 36  
 Eldridge J. J., Izzard R. G., Tout C. A., 2008, *MNRAS*, 384, 1109  
 Elias-Rosa N., et al., 2011, *ApJ*, 742, 6  
 Elias-Rosa N., et al., 2010, *ApJ*, 714, L254  
 Ergon M., et al., 2014, *arXiv*, arXiv:1408.0731  
 Falk S. W., Arnett W. D., 1977, *ApJS*, 33, 515  
 Faran T., et al., 2014a, *MNRAS*, 442, 844  
 Faran T., et al., 2014b, *MNRAS*, 445, 554  
 Filippenko A. V., 1997, *ARA&A*, 35, 309  
 Folatelli G., et al., 2014, *ApJ*, 793, L22  
 Gall E. E. E., et al., 2015, *arXiv*, arXiv:1502.06034  
 Goldfriend T., Nakar E., Sari R., 2014, *arXiv*, arXiv:1404.6313



- González-Gaitán S., et al., 2015, MNRAS, 451, 2212
- Grassberg E. K., Imshennik V. S., Nadyozhin D. K., 1971, Ap&SS, 10, 28
- Hachisu I., Matsuda T., Nomoto K., Shigeyama T., 1990, ApJ, 358, L57
- Hamuy M., 2003, ApJ, 582, 905
- Holoien T. W.-S., et al., 2014, arXiv, arXiv:1411.3322
- Inserra C., et al., 2013, A&A, 555, A142
- Jerkstrand A., Ergon M., Smartt S. J., Fransson C., Sollerman J., Taubenberger S., Bersten M., Spyromilio J., 2015, A&A, 573, A12
- Kasen D., Woosley S. E., 2009, ApJ, 703, 2205
- Kuncarayakti H., et al., 2013, AJ, 146, 31
- Litvinova I. I., Nadezhin D. K., 1983, Ap&SS, 89, 89
- Maund J. R., Fraser M., Reilly E., Ergon M., Mattila S., 2015, MNRAS, 447, 3207
- Mcley L., Soker N., 2014, MNRAS, 445, 2492
- Meynet G., et al., 2015, A&A, 575, A60
- Moriya T. J., 2014, A&A, 564, A83
- Moriya T. J., Maeda K., Taddia F., Sollerman J., Blinnikov S. I., Sorokina E. I., 2013, MNRAS, 435, 1520
- Morozova V., Piro A. L., Renzo M., Ott C. D., Clausen D., Couch S. M., Ellis J., Roberts L. F., 2015, arXiv, arXiv:1505.06746
- Nomoto K. I., Iwamoto K., Suzuki T., 1995, PhR, 256, 173
- Nomoto K., Maeda K., Tanaka M., Suzuki T., 2011, Ap&SS, 336, 129
- Paxton B., Bildsten L., Dotter A., Herwig F., Lesaffre P., Timmes F., 2011, ApJS, 192, 3
- Paxton B., et al., 2015, arXiv, arXiv:1506.03146
- Paxton B., et al., 2013, ApJS, 208, 4
- Pejcha O., Prieto J. L., 2015a, ApJ, 806, 225
- Pejcha O., Prieto J. L., 2015b, ApJ, 799, 215
- Popov D. V., 1993, ApJ, 414, 712
- Poznanski D., 2013, MNRAS, 436, 3224
- Poznanski D., Kostrzewa-Rutkowska Z., Wyrzykowski L., Blagorodnova N., 2015, MNRAS, 449, 1753
- Quataert E., Shiode J., 2012, MNRAS, 423, L92
- Sanders N. E., et al., 2015, ApJ, 799, 208
- Smartt S. J., 2009, ARA&A, 47, 63
- Shigeyama T., Nomoto K., 1990, ApJ, 360, 242
- Shigeyama T., Suzuki T., Kumagai S., Nomoto K., Saio H., Yamaoka H., 1994, ApJ, 420, 341
- Suntzeff N. B., Phillips M. M., Elias J. H., Walker A. R., Depoy D. L., 1992, ApJ, 384, L33
- Swartz D. A., Wheeler J. C., Harkness R. P., 1991, ApJ, 374, 266
- Tominaga N., et al., 2015, ApJ, submitted
- Utrobin V. P., 2007, A&A, 461, 233
- Utrobin V. P., Chugai N. N., 2013, A&A, 555, A145
- Utrobin V. P., Wongwathanarat A., Janka H.-T., Müller E., 2015, A&A, 581, A40
- Valenti S., et al., 2015, MNRAS, 448, 2608
- Vink J. S., de Koter A., Lamers H. J. G. L. M., 2001, A&A, 369, 574
- Wheeler J. C., Johnson V., Clocchiatti A., 2015, MNRAS, 450, 1295
- Woosley S. E., 1988, ApJ, 330, 218
- Woosley S. E., Eastman R. G., Weaver T. A., Pinto P. A., 1994, ApJ, 429, 300
- Young T. R., 2004, ApJ, 617, 1233
- Young T. R., Smith D., Johnson T. A., 2005, ApJ, 625, L87